Prolonged Lifetimes of Histologic Autofluorescence in Ectopic Retinal Pigment Epithelium in Age-Related Macular Degeneration

Rowena Simon,[1] Marius Jentsch,[1] Parva Karimimousivandi,[1] Dongfeng Cao,[2] Jeffrey D. Messinger,[2] Daniel Meller,[1] Christine A. Curcio,[2] and Martin Hammer[1,3]

[1]Department of Ophthalmology, University Hospital Jena, Jena, Germany
[2]Department of Ophthalmology and Visual Sciences, School of Medicine, University of Alabama at Birmingham, Birmingham, Alabama, United States
[3]Center for Medical Optics and Photonics, University of Jena, Jena, Germany

Correspondence: Rowena Simon, University Hospital Jena, Department of Ophthalmology, Am Klinikum 1, 07747 Jena, Germany; rowena.simon@med.uni-jena.de.

Received: June 16, 2022
Accepted: November 4, 2022
Published: December 5, 2022

Citation: Simon R, Jentsch M, Karimimousivandi P, et al. Prolonged lifetimes of histologic autofluorescence in ectopic retinal pigment epithelium in age-related macular degeneration. *Invest Ophthalmol Vis Sci.* 2022;63(13):5. https://doi.org/10.1167/iovs.63.13.5

Purpose. The purpose of this study was to investigate histologic autofluorescence lifetimes and spectra of retinal pigment epithelium (RPE) on the transition from normal aging to RPE activation and migration in age-related macular degeneration (AMD).

Methods. Autofluorescence lifetimes and spectra of 9 donor eyes were analyzed in cryosections by means of 2-photon excited fluorescence at 960 nm. Spectra were detected at 483 to 665 nm. Lifetimes were measured using time-correlated single photon counting in 2 spectral channels: 500 to 550 nm (short-wavelength spectral channel [SSC]) and 550 to 700 nm (long-wavelength spectral channel [LSC]). Fluorescence decays over time were approximated by a series of three exponential functions. The amplitude-weighted mean fluorescence lifetime was determined. Markers for retinoid activity (RPE65) and immune function (CD68) were immunolocalized in selected neighboring sections.

Results. We identified 9 RPE morphology phenotypes resulting in 399 regions of interest (ROIs) for spectral and 497 ROIs for lifetime measurements. RPE dysmorphia results in a shorter wavelength peak of spectral emission: normal aging versus RPE migrated into the retina (intraELM) = 601.7 (9.5) nm versus 581.6 (7.3) nm, $P < 0.001$, whereas autofluorescence lifetimes increase: normal aging versus intraELM: SSC 180 (44) picosecond (ps) versus 320 (86) ps, $P < 0.001$; and LSC 250 (55) ps versus 441 (76) ps, $P < 0.001$. Ectopic RPE within the neurosensory retina is strongly CD68 positive and RPE65 negative.

Conclusions. In the process of RPE degeneration, comprising different steps of dysmorphia and migration, lengthening of autofluorescence lifetimes and a hypsochromic shift of emission spectra can be observed. These autofluorescence changes might provide early biomarkers for AMD progression and contribute to our understanding of RPE-driven pathology.

Keywords: age-related macular degeneration (AMD), retinal pigment epithelium (RPE), fundus autofluorescence (FAF), fluorescence lifetime, fluorescence spectra, atrophy, migration

Age-related macular degeneration (AMD) is the leading cause of legal blindness in high income countries in individuals >55 years of age.[1,2] AMD is characterized by accumulation of extracellular deposits, of which drusen are the best studied, along with progressive degeneration of choriocapillaris endothelium, retinal pigment epithelium (RPE), and photoreceptors. RPE dysmorphia, indicative of pathologic activation, is a key symptom of AMD.

Hyper-reflective foci (HRF) within the neurosensory retina are a well-documented optical coherence tomography (OCT) biomarker for AMD progression risk.[3–6] HRF are also associated with hyperautofluorescent signals in fundus autofluorescence (FAF) imaging,[7] a widely used imaging technique in the diagnosis and management of AMD.[8,9] The development of fluorescence lifetime imaging ophthalmoscopy (FLIO) enabled the characterization of FAF signals by fluorescence lifetimes[10–12] and spectral emission.[7,13,14] We recently described a lengthening of FAF lifetimes and a hypsochromic (blue) shift of emission spectra observed by FLIO in the process of RPE degeneration,[7] comprising different steps of dysmorphia, hyperpigmentation, and anterior migration.[15–17] However, a variety of fluorophores can contribute to the signal, and FLIO measurements cannot resolve single molecules. FLIO signals represent the overall state of tissue, comprising all retinal layers, at each pixel in the projection image.[18] Because both FAF and FLIO provide en face images without depth resolution, autofluorescence from different fundus layers is summed in these signals. This superposition of different fluorophores from different anatomic structures make it difficult to distinguish and char-

acterize them. Therefore, insight in fluorescence contributions from these structures, fundus layers, and single cells undergoing pathologic alteration can be gained if in vivo observations are complemented by histological studies.

In this study, we measured autofluorescence spectra and lifetimes of normal aged as well as activated and dysmorphic RPE cells in cryosections of donor eyes to verify our in vivo data. This information, along with immunohistochemical staining of functional cell markers, could elucidate high value autofluorescence characteristics in the development or progression of AMD.

Methods

Human Donor Tissue

Use of human tissue was approved by the Institutional Review Board at the University of Alabama at Birmingham (#N170213002). Whole eyes of Caucasian donors aged 80 years or older without diabetes mellitus and no reported history of head trauma, surgeries affecting the retina, or conditions affecting the macula other than AMD were collected within 6 hours of death from Advancing Sight Network (Birmingham, AL, USA). After anterior segment removal, eyes were preserved in 4% buffered paraformaldehyde and screened for AMD using ex vivo multimodal imaging (by authors J.D.M. and C.A.C.), including OCT and histology, as described.[19,20] Following postmortem fundus inspection and histologic review, eyes with pathologic features of AMD, including RPE damage and translocation in the macula region, were selected for further analysis. Unstained glass slides with 12-µm thick cryosections were shipped on dry ice by overnight courier to Jena for autofluorescence spectral and lifetime microscopy (3-4 slides per eye). The right eyes of nine donors (mean age = 86.7 ± 6.7 years, women $n = 6$ and men $n = 3$) were used in this study. Selected segments of the RPE cell layer were imaged. Selection criteria for imaging included sections of obvious changes in RPE morphology (pre-screened by epifluorescence microcopy, $\lambda = 480$ nm, Inverted Microscope Eclipse TS100 equipped with a CFI Achromat LWD ADL20x/0.40NA objective, Nikon, Japan) and random areas without obvious RPE dysmorphia selected from slides of the same donor.

Immunohistochemistry

Detailed methods for immunohistochemistry are available elsewhere.[17,20] The tissues used for this study were embedded in carboxymethylcellulose for parallel studies using imaging spectrometry. Our previous immunohistochemical results used sections embedded in polyethylene glycol. These two preparation techniques can give different immunohistochemistry signals depending on the antibody and thus it was important to repeat our previous findings of molecular transdifferentiation on tissues used for fluorescence lifetime microscopy. Markers for retinoid activity (RPE65, an isomerohydrolase of the classic visual cycle) and immune function (CD68, a lysosome protein common in macrophages) were localized in sections using an avidin-biotin-peroxidase detection system and red reaction product (AEC, 3-amino-9-ethylcarbozole). Briefly, after antigen retrieval and blocking steps, cryosections were immunoprobed with primary antibodies, both from Thermo Fisher Scientific (Waltham, MA, USA) directed against CD68 (MA1-80133) and RPE65 (MA-1-16578), followed by incubation with horse anti-mouse/rabbit secondary antibody (Vector Labs, Cat# PK-7200, Newark, CA, USA). To reveal cell nuclei, sections were stained with hematoxylin solution (PASH kit, Poly Scientific R&D Corp., Bay Shore, NY, USA; #K047). Glass slides were scanned using a microscope with a robotic stage (Olympus VSI 120, CellSens; Olympus, Center Valley, PA, USA) and 20× and 40× objectives.

Spectral and Fluorescence Lifetime Imaging Microscopy

Autofluorescence spectra and lifetimes were recorded using an inverted multiphoton laser scanning microscope (Axio Observer Z.1 and LSM 710 NLO, 63x oil immersion objective Plan-Apochromat NA = 1.4; Carl Zeiss, Jena, Germany) in combination with a femtosecond Ti:Sapphire laser (Chameleon Ultra, Coherent Inc., Santa Clara, CA, USA; repetition rate of 80 MHz with a pulse duration of 140 fs) and a single photon counting fluorescence lifetime imaging setup (Becker & Hickl GmbH, Berlin, Germany) with a 20 to 30 picosecond (ps) time resolution, as described.[19] The excitation wavelength for spectral and lifetime recordings was set to 960 nm for two-photon excitation (TPE).

All spectral images were recorded as an average of 100 fast scans (pixel dwell time of 1.6 µs) with a resolution of 512 × 512 pixel and a field of view of 224.92 µm × 224.92 µm. The spectral QUASAR detector of the LSM 710 was used for spectral imaging. The autofluorescence emission was recorded in the range of 483 to 665 nm with a spectral resolution of 9.6 nm.

The lifetime imaging measurements are based on the principle of time-correlated single photon counting (TCSPC). The two-photon-excited fluorescence was recorded in two spectral channels. The short-wavelength spectral channel (SSC) was 500 to 550 nm, and the long-wavelength spectral channel (LSC) was 550 to 700 nm. All fluorescence lifetime imaging microscopy (FLIM) images were acquired as an average of 100 fast scans (mean photon count per pixel of approximately 1000, pixel dwell time of 3.1 µs) with a resolution of 256 × 256 pixel and a field of view of 96.4 × 96.4 µm.

The fluorescence decay images from the FLIM detectors were analyzed using the software SPCImage 8.0 (Becker&Hickl GmbH, Berlin, Germany). For decay data fitting, a 3 × 3 pixel binning was applied. The decays where approximated by the fitting method of weighted least chi-squares and with a three-exponential model yielding three decay time constants and three amplitudes.

Data Analysis

Different RPE morphologies located in and near the macula region were identified in bright field images and autofluorescence intensity images of unstained sections. A series of RPE morphologies were originally categorized in sub-micrometer epoxy-resin histology by Zanzottera et al.[15,16] and Curcio et al.[6] using cell shape, organelle content, and location with respect to the native RPE layer. In these prior studies, RPE morphologies were assembled into hypothesized progression sequences, of which the best documented is shown in Figure 1. These classifications have also been used in 12 to 14 µm thick cryosections like those used here.[17] We use original names of the RPE phenotypes, including uniform and slightly nonuniform segments (collectively denoted as

Investigative Ophthalmology & Visual Science

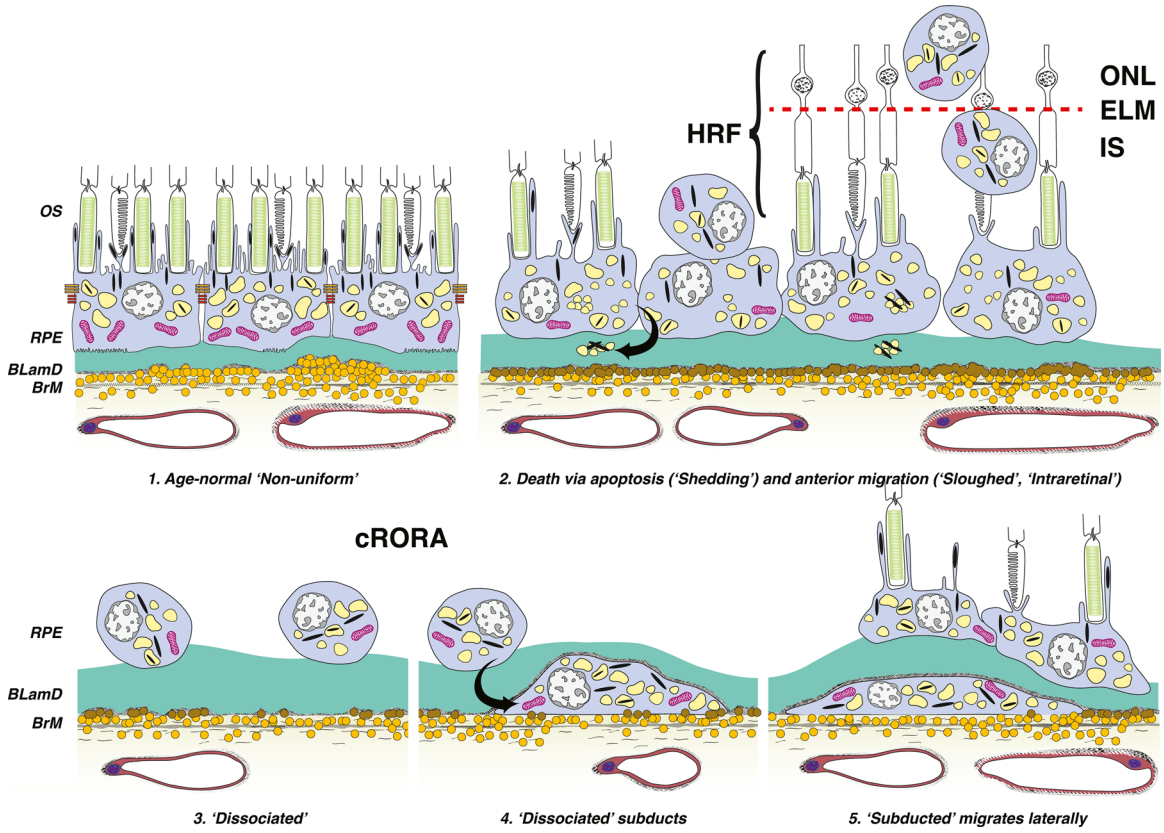

Figure 1. Schematic for cRORA in nonneovascular AMD, adapted from Zanzottera et al.,[16] and Cao et al.,[17] © 2016 by Ophthalmic Communications Society, Inc. Six morphologic phenotypes of RPE from a system of 15 are shown. (1) Age-normal "non-uniform" RPE overlies Bruch's membrane (BrM), which has abundant lipoprotein particles (*yellow*). Basal laminar deposit (BLamD, *green*) is thickened basement membrane material between the RPE cell body and native RPE basal lamina. RPE organelles are melanosomes (*black*), lipofuscin (*yellow*), and mitochondria (*pink*). (2) Anteriorly migrated "sloughed" and "intraretinal" (intraPS and intraELM) RPE manifest clinically as HRF. "Shedding" cells release organelle clusters (*curved arrow*) basally into BLamD, thought to represent apoptosis. (3) Due to cell death and migration, the RPE layer disintegrates. "Dissociated" RPE are fully pigmented, nucleated cells scattered in the atrophic zone. BLamD persists after RPE death. (4) "Subducted" cells containing RPE organelles, appearing to originate from dissociated cells (*arrow*), are flattened against BrM. (5) "Subducted" cells migrate outside the atrophic area. OS, outer segments of photoreceptors; IS, inner segments of photoreceptors; RPE, retinal pigment epithelium; HRF, hyperreflective foci; ELM, external limiting membrane; ONL, outer nuclear layer.

"normal aging"), very nonuniform RPE, dissociated RPE (scattered across atrophic areas), bilaminar RPE (2 layers of fully pigmented RPE cells), subducted RPE cells, and shedding RPE.

In this report, the original stages of sloughed RPE (RPE cells released into the subretinal space) and intraretinal RPE (pigmented cells within the neurosensory retina) were further divided (see Fig. 1). Migration depth into the retina is considered a sign of chronicity and more advanced pathology.[5,21] We wished to test whether cells at different migration depths exhibited different autofluorescence characteristics. This report (see Fig. 1) accordingly separates sloughed RPE (RPE cells released into the subretinal space, but still with contact to the RPE monolayer), RPE cells located next to the photoreceptor inner or outer segments without contact to the RPE monolayer (intraPS), and RPE cells migrated anteriorly beyond the external limiting membrane into neurosensory retina (intraELM). Regions of interests (ROIs) were encircled in spectral and lifetime recordings using the respective software tools.

For each spectral image, ROIs were defined by authors P.K. and R.S. in the software ZEN Black 2.3 (Carl Zeiss Microscopy GmbH, Jena, Germany) and the averaged spectrum per ROI exported and used for further analysis with OriginPro (OriginPro version 9.1; MicroCalLLC/GE Healthcare, Piscataway, NJ, USA). To compare emission spectra between different RPE morphologies, spectra were normalized to 1 by dividing all intensity values by the corresponding maximum intensity value. The normalized spectra were analyzed using a curve-fitting algorithm, and a fifth order polynomial function was applied. The fitting program uses the Marquardt–Levenberg algorithm that finds the true absolute minimum value of the sum of squared deviations (the value of chi-square) by an iterative process. The quality of fitting was determined by the random spread in residuals of fitting, correlation coefficient r^2, and low chi-square values; the latter two being the more weighted factors. After fitting, the resulting fitting curves were numerically integrated using the trapezoidal rule to precisely determine the emission maximum wavelength (EMW) and bandwidth (full width at half-maximum [FWHM]) of the spectra for different cell morphologies and localizations. These values were used for statistical analysis.

The autofluorescence lifetime data were fitted in SPCImage, as described above, and the results imported into the software FLIMX, which is documented elsewhere[22] and

Investigative Ophthalmology & Visual Science

freely available under the open-source BSD license (http://www.flimx.de). ROIs defined by RPE morphology were outlined by authors M.J. and R.S. on the fluorescence intensity images to avoid bias by color-coded lifetimes. The amplitude-weighted mean decay time τ_m as well as the relative abundances $\alpha\%_{1\text{-}3}$ of single decay components with time constants $\tau_{1\text{-}3}$ were exported per ROI and used for statistical analysis. The resulting images are color-coded, depicting shorter lifetimes in red and longer lifetimes in blue.

Statistical Analysis

SPSS 22 (IBM, SPSS Inc., Chicago, IL, USA) was used for all statistical analysis. The Kruskal-Wallis test was used for comparing autofluorescence spectra and lifetime parameters between different RPE morphologies. For pairwise comparisons, adjusted significance levels are given after multiplying the unadjusted significance values by the number of comparisons (Dunn-Bonferroni post hoc test). The effect size is given as *r* value derived from the z-value (standard test statistic) divided by the root of the sample size. Due to low sample size, subducted and shedding RPE[6,23] were excluded from pairwise comparisons, and only descriptive statistics are reported. All numerical results are given as median (interquartile range [IQR]) in the text as well as in tables if not stated otherwise.

Results

RPE Cell/Layer Morphology Phenotypes (ROIs)

Due to different field-of-view settings between spectral and lifetime imaging, the number of samples per morphology group varies. ROIs in spectral images sometimes cover multiple ROIs in lifetime images. Overall, on 23 slices of 9 donor eyes, for spectral imaging 399 RPE locations (ROIs) were

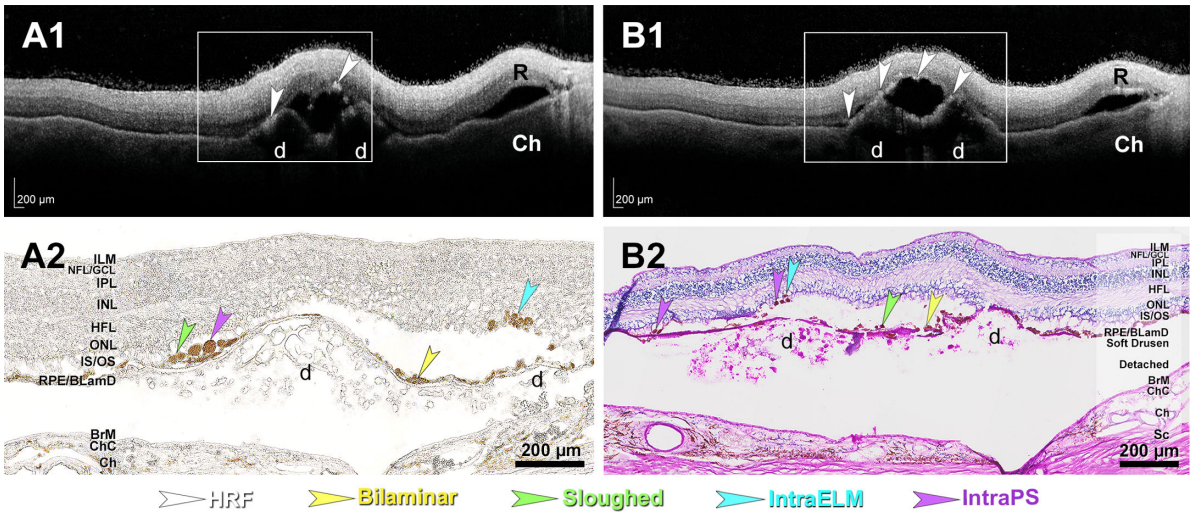

Figure 2. Hyperreflective foci (HRF) in ex vivo optical coherence tomography (OCT) correspond to ectopic RPE on histology. (**A1, B1**) HRFs (*white arrowheads*) are visible in this retina of a 90-year-old white female donor by ex vivo OCT. Areas in frames are magnified in A2 and B2. (**A2**) RPE phenotypes corresponding to HRF are visible in unstained sections. (**B2**) RPE phenotypes corresponding to HRF are visible in a section stained with periodic acid–Schiff hematoxylin. R, retina; d, soft drusen; ILM, internal limiting membrane; NFL, nerve fiber layer; GCL, ganglion cell layer; IPL, inner plexiform layer; INL, inner unclear layer; HFL, Henle fiber layer; ONL, outer nuclear layer; IS, inner segments of photoreceptors; OS, outer segments of photoreceptors; RPE, retinal pigment epithelium; BLamD, basal laminar deposit; BrM, Bruch's membrane; ChC, choriocapillary; Ch, choroid; Sc, sclera; intraPS, ectopic RPE next to photoreceptor inner or outer segments; intraELM, ectopic RPE within the retina after crossing the external limiting membrane.

Table 1. EMW and FWHM for Nine RPE Morphology Phenotypes

		EMW [nm]			FWHM [nm]		
	n	Median	IQR	*P* vs. Normal Aging	Median	IQR	*P* vs. Normal Aging
Normal aging	64	601.7	9.5		187.4	18.5	
Very nonuniform	116	590.5	5.6	**<0.001**	188.9	17.7	1.000
Sloughed	18	589.5	8.3	**0.002**	181.7	14.2	1.000
IntraPS	52	585.5	8.3	**<0.001**	178.3	11.0	**0.002**
IntraELM	97	581.6	7.3	**<0.001**	171.7	12.4	**<0.001**
Bilaminar	22	593.5	7.0	0.206	189.2	7.5	1.000
Dissociated	22	590.3	3.7	**<0.001**	185.8	13.2	1.000
Subducted	5	583.6	4.7	—	174.0	14.7	—
Shedding	3	597.2		—	187.8		—

Changes in RPE morphology are accompanied by a shortening and narrowing of the autofluorescence emission after TPE excitation at 960 nm. *n* = number of ROIs, results are given as median with interquartile range (IQR). Statistic by Kruskal-Wallis with Dunn-Bonferroni post hoc test. Corrected *P* values for comparison against normal aged RPE are given. EMW, emission maximum wavelength; FWHM, full width at half-maximum.

Investigative Ophthalmology & Visual Science

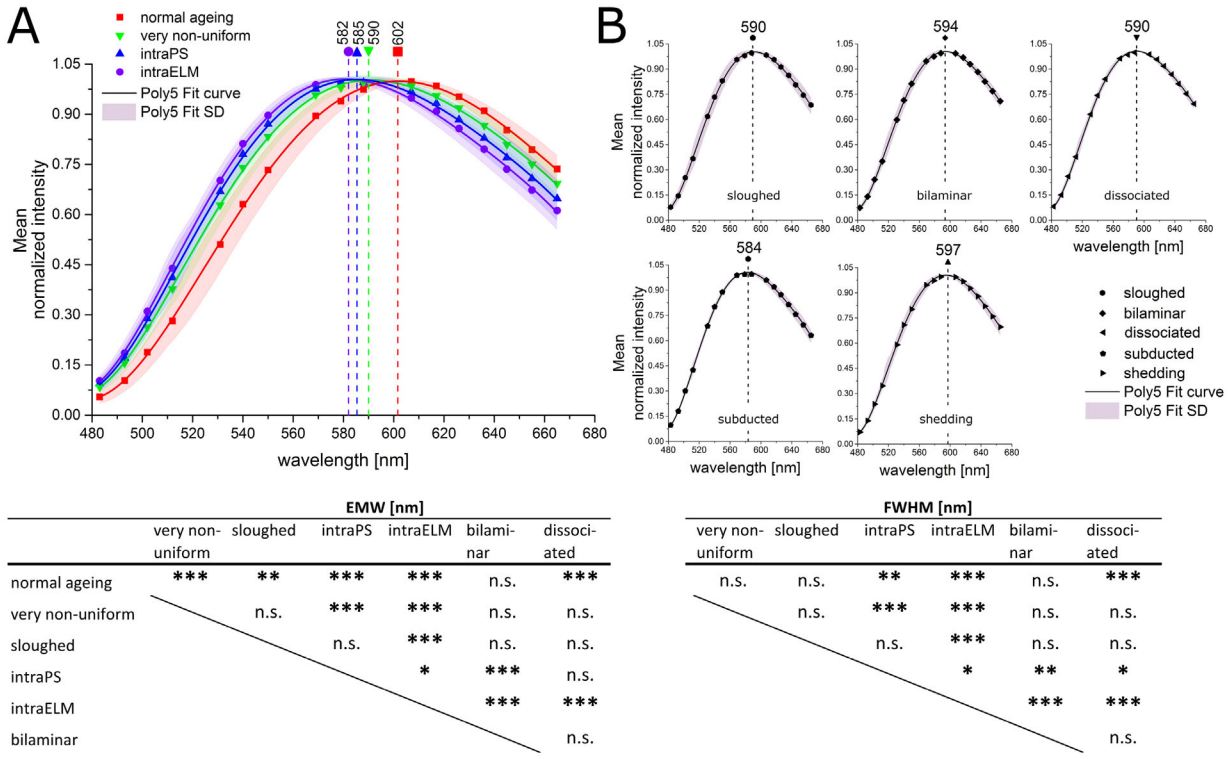

EMW [nm]

	very non-uniform	sloughed	intraPS	intraELM	bilaminar	dissociated
normal ageing	***	**	***	***	n.s.	***
very non-uniform		n.s.	***	***	n.s.	n.s.
sloughed			n.s.	***	n.s.	n.s.
intraPS				*	***	n.s.
intraELM					***	***
bilaminar						n.s.

FWHM [nm]

	very non-uniform	sloughed	intraPS	intraELM	bilaminar	dissociated
normal ageing	n.s.	n.s.	**	***	n.s.	***
very non-uniform		n.s.	***	***	n.s.	n.s.
sloughed			n.s.	***	n.s.	n.s.
intraPS				*	**	*
intraELM					***	***
bilaminar						n.s.

Figure 3. Comparison of spectral characteristics of different RPE morphologies (**A**). RPE cells with uniform layer morphology (normal aging, *red*), very nonuniform RPE cell layer (*green*), and ectopic RPE intraretinal in the photoreceptor layer (intraPS, *blue*), or after crossing the external limiting membrane (intraELM, *violet*). (**B**) sloughed RPE released into the subretinal space, dissociated RPE in atrophic areas, bilaminar RPE, subducted RPE cells and shedding RPE. Averaged fluorescence emission spectra of RPE cells and clusters imaged on histologic slices (mean) and the corresponding Poly5 fit curve (mean ± SD) are depicted. The excitation wavelength was 960 nm (TPE), emission spectra was normalized to the peak emission intensity, *dasbed lines* mark the emission maximum wavelength (EMW) per morphology. EMW, emission maximum wavelength; FWHM, full width at half-maximum, statistic by Kruskal-Wallis with Dunn-Bonferroni post hoc test. ***$P < 0.001$; **$P < 0.01$; *$P < 0.05$.

examined. For lifetime measurements, 497 ROIs were studied. Two eyes had the most prominent occurrence of RPE dysmorphia, accounting for two-thirds of all ROIs analyzed in this study. These two eyes were diagnosed with intermediate AMD by expert inspection of postmortem fundus and ex vivo OCT followed by histology. Further eyes were diagnosed with early AMD ($n = 4$) and atrophic ($n = 1$). Two unremarkable eyes with no obvious RPE changes relatable to AMD within in the macula region were included as well to cover a wide range of RPE morphologies. We identified nine different phenotypes of RPE cell morphologies following the classification given by Zanzottera et al.[15,16] and Curcio et al.[6], modified as described in the Methods. These include normal aged RPE cells (spectral/lifetime ROIs: $n = 64/112$), very nonuniform RPE cells ($n = 166/133$), sloughed RPE cells ($n = 18/21$), intraPS ($n = 52/63$), intraELM ($n = 97/109$), dissociated RPE cells ($n = 22/27$), bilaminar RPE cells ($n = 22/24$), and very few subducted RPE cells

Table 2. Prolongation of Autofluorescence Lifetime in Ectopic RPE

		τm SSC [ps]				τm LSC [ps]			
	n	**Median**	**IQR**	***P* vs. Normal Ageing**	**Effect Size r**	**Median**	**IQR**	***P* vs. Normal Ageing**	**Effect Size r**
Normal aging	112	180	44			250	55		
Very nonuniform	133	226	51	**<0.001**	0.47	317	43	**<0.001**	0.51
Sloughed	21	243	89	**<0.001**	0.44	362	104	**<0.001**	0.49
IntraPS	63	302	73	**<0.001**	0.88	395	80	**<0.001**	0.92
IntraELM	109	320	86	**<0.001**	1.10	441	76	**<0.001**	1.19
Bilaminar	24	230	36	**0.001**	0.35	310	25	**0.001**	0.35
Dissociated	27	218	42	**0.023**	0.28	328	37	**<0.001**	0.43
Subducted	5	376	154	—		480	123	—	
Shedding	3	230		—		313		—	

Changes in RPE morphology are accompanied by a prolongation of mean autofluorescence lifetime (τ_m) after TPE excitation at 960 nm. n = number of ROIs, results are given as median with interquartile range (IQR). Statistic by Kruskal-Wallis with Dunn-Bonferroni post hoc test. Corrected P values for normal aged RPE are indicated. SSC, short-wavelength spectral channel (500-550 nm); LSC, long-wavelength spectral channel (550-700 nm).

Investigative Ophthalmology & Visual Science

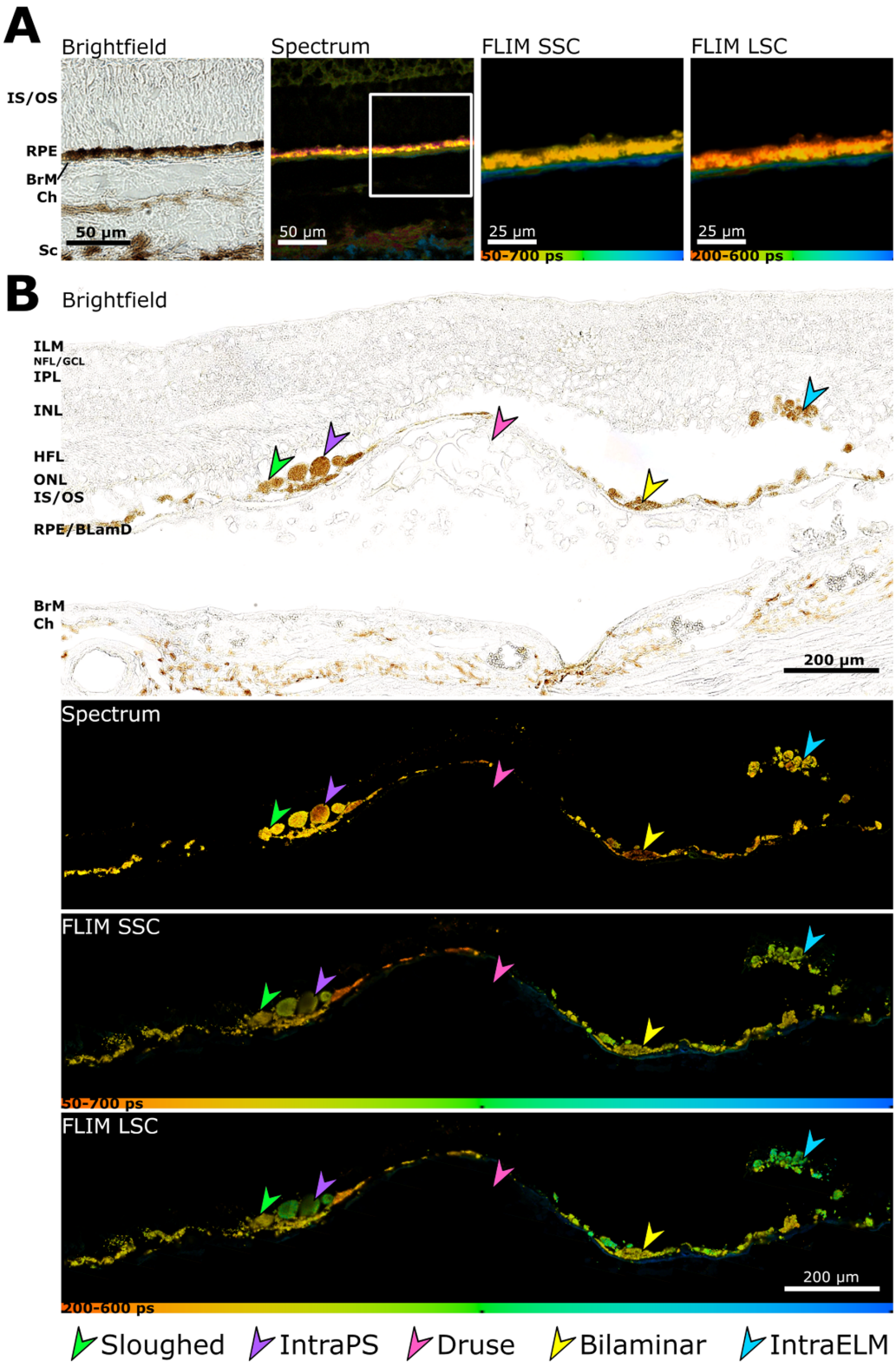

Figure 4. Ectopic RPE shows a prolongation in autofluorescence lifetime. (**A**) Brightfield, spectral emission and autofluorescence lifetimes (τm) in SSC and LSC (pseudo-colored) for normal aged RPE. (**B**) Brightfield, spectral emission and autofluorescence lifetimes (τm) in SSC and LSC for four different RPE morphologies. *Pink arrowhead*, soft druse; *yellow arrowhead*, bilaminar RPE; *bright green arrowhead*, sloughed RPE; *purple arrowhead*, ectopic RPE next to photoreceptor inner or outer segments (intraPS); *blue arrowhead*, ectopic RPE within the retina after crossing the external limiting membrane (intraELM). Scale bars as indicated.

Investigative Ophthalmology & Visual Science

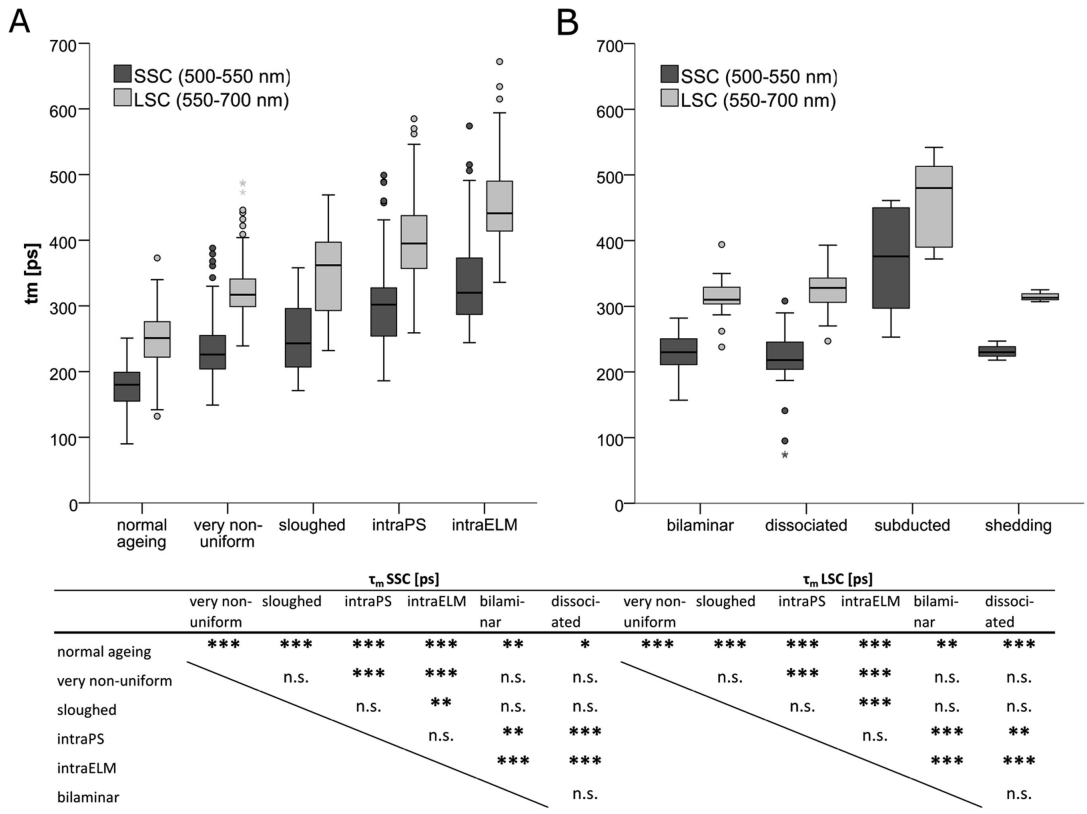

Figure 5. Boxplot showing the prolongation of mean autofluorescence lifetimes (τm) for ectopic RPE. (**A**) RPE cells with uniform layer morphology (normal aging), very nonuniform RPE cell layer, sloughed RPE released into the subretinal space, and ectopic RPE intraretinal in the photoreceptor layer (intraPS) or after crossing the external limiting membrane (intraELM). (**B**) Bilaminar RPE, dissociated RPE in atrophic areas, subducted RPE cells and shedding RPE. The excitation wavelength was 960 nm (TPE), statistic by Kruskal-Wallis with Dunn-Bonferroni post hoc test. ***$P < 0.001$; **$P < 0.01$; *$P < 0.05$.

($n = 5$) or shedding RPE cells ($n = 3$; see Figs. 1, 2). The density of pigmentation was not a criterion for classification; however, all analyzed cells were pigmented as well as autofluorescent.

Autofluorescence Emission Spectra

Compared to normal aged RPE cells, dysmorphic RPE cells emit at a shorter wavelengths χ^2 (6, $N = 391$) = 238.15, $P < 0.001$. The EMW is reduced from 601.7 (9.5) nm in normal aged to 590.5 (5.6) nm for very nonuniform RPE cells ($P < 0.001$). No significant differences in fluorescence emission spectra were found between very nonuniform and sloughed or between sloughed and intraPS RPE cells/cell clusters. However, emission had even shorter wavelengths for RPE cells at different stages of migration into the retina (very nonuniform versus intraPS and intraELM: 590.5 [5.6] nm versus 585.5 [8.3] nm and 581.6 [7.3] nm, $P < 0.001$ for both; sloughed versus intraELM: 589.5 [8.3] nm versus 581.6 [7.3] nm, $P < 0.001$; intraPS versus intraELM: $P = 0.022$; Table 1, Fig. 3; for medians of EMW per cell entity, averaged over all cells per subject, see Supplementary Table S3).

Furthermore, the spectral emission is narrower for ectopic RPE located within the retina, as seen by a decrease in the FWHM, χ^2 (6, $N = 391$) = 119.11, $P < 0.001$ (see Table 1). The FWHM decreased from 187.4 (18.5) nm in normal aged RPE cells to 178.3 (11) nm for intraPS RPE cells ($P = 0.002$). No significant differences were found among normal aged, very nonuniform, and sloughed RPE cells. However, the FWHM further decreased for RPE cells advancing into the retina (intraPS versus intraELM: 178.3 [11] nm versus 171.7 [12.7] nm, $P = 0.045$).

Autofluorescence Lifetimes

The autofluorescence mean lifetimes in both spectral channels over all ROIs increased with severity of RPE dysmorphia (Fig. 4), SSC: χ^2 (6, $N = 490$) = 308.41, $P < 0.001$, and LSC: χ^2 (6, $N = 490$) = 354.34, $P < 0.001$ (Table 2, Fig. 5, for medians of lifetimes per cell entity, averaged over all cells per subject, see Supplementary Table S3). Especially RPE cells/cell clusters that had deeply penetrated into the retina were found to have markedly lengthened lifetimes compared to normal aged cells (normal aging versus intraELM: SSC = 180 [44] ps versus 320 [86] ps, $P < 0.001$, effect size $r = 1.10$; LSC = 250 [55] ps versus 441 [76] ps, $P < 0.001$, $r = 1.19$). The most pronounced lengthening of lifetimes was observed for subducted RPE (SSC = 376 [154] ps and LSC = 480 [123] ps). Only a few subducted cells were analyzed, and no statistical comparison was performed.

Very nonuniform and sloughed RPE cells/cell clusters did not differ in lifetimes from each other, whereas intraPS and intraELM were significantly longer compared to very nonuniform RPE cells ($P < 0.001$ for both in SSC and LSC). IntraELM RPE cells, but not intraPS RPE cells, also showed prolonged lifetimes compared to sloughed cells (SSC: $P = 0.001$ and

Investigative Ophthalmology & Visual Science

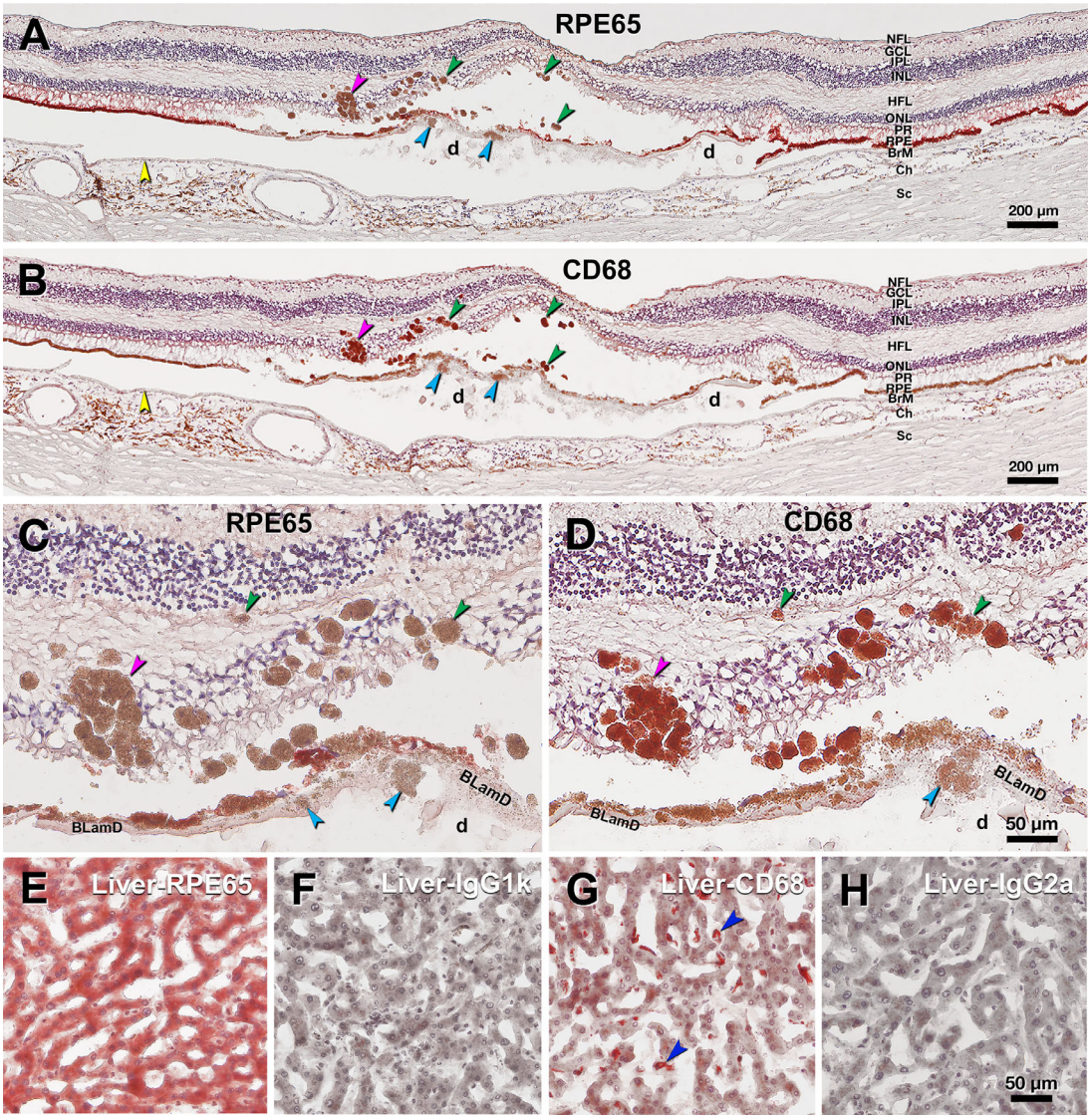

Figure 6. Immunohistochemistry contrasts ectopic and orthotopic RPE in age-related macular degeneration. This retina of a 90-year-old white female donor has huge soft drusen and continuous basal laminar deposit (BLamD) under the fovea. *Yellow arrowheads*, Bruch's membrane. Scale bars apply to each row. (**A**) RPE65 immunoreactivity of ectopic RPE including sloughed/intraretinal phenotypes presenting as hyper-reflective foci (HRF) at *green/pink* (RPE plume) *arrowheads* and shedding RPE phenotype at *cyan arrowhead*. (**B**) CD68 immunoreactivity of ectopic RPE including sloughed/intraretinal phenotypes at *green/pink* (RPE plume) *arrowheads* and shedding RPE phenotype at *cyan arrowhead* in the same retina in panel **A**. (**C**) Magnified view of ectopic RPE lacking RPE65 immunoreactivity in panel **A**. (**D**) Magnified view of CD68 immunoreactive ectopic RPE in panel **B**. (**E-G**) Human liver tissue. **E** RPE65 positive control. **F** Sham control for RPE65. **G** CD68 positive control, blue arrowheads indicate CD68+ Kupffer cells. (**H**) Sham control for CD68. d, soft drusen; BLamD, basal laminar deposit; NFL, nerve fiber layer; GCL, ganglion cell layer; IPL, inner plexiform layer; INL, inner unclear layer; HFL, Henle fiber layer; ONL, outer nuclear layer; PR, photoreceptor layer; RPE, retinal pigment epithelium; BrM, Bruch's membrane; Ch, choroid; Sc, sclera.

LSC: $P < 0.001$). The mean lifetimes in the SSC and LSC did not differ between intraPS and intraELM RPE cells/cell clusters. Autofluorescence lifetime data were best fitted with a series of three exponential functions. Considering single decay components can give more detailed information than t_m only. Whereas t_m was not significantly different for intraPS and intraELM, they differed in the abundance of the single decay components α%1 (SSC = 77.7 [5.2] % vs. 75.4 [4.7] %, $P = 0.047$; LSC = 72.6 [6.8] % vs. 69.8 [5.8] %, $P = 0.007$), α%2 (LSC = 24.0 [4.3] % vs. 26.0 [3.6] %, $P = 0.005$), and α%3 (SSC = 2.0 [1.6] % vs. 2.8 [1.4] %, $P = 0.021$; and LSC = 3.3 [1.7] % vs. 4.1 [2.0] %, $P = 0.007$; Supplementary Tables S1, S2).

Immunohistochemistry

AMD eyes with HRF by ex vivo OCT exhibited pigmented cells in the outer nuclear layer and Henle fiber layer by histology (Figs. 2, 6). Neighboring slides from the same donor used for fluorescence lifetimes showing comparable RPE morphology as those imaged for spectral characterization were immunoprobed for markers for retinoid and immune functions (RPE65 and CD68, respectively). Fully pigmented ectopic RPE within the neurosensory retina, as well as individual sloughed cells, were strongly positive for CD68 immunoreactivity and negative for RPE65 (see Fig. 6).

Investigative Ophthalmology & Visual Science

Discussion

Our most important result is that RPE cells in a recently proposed morphologic progression sequence from normal aging to dysmorphic including intraretinal[15,17] (see Fig. 1), gradually show longer lifetimes and shorter emission wavelengths.

This study extends our previous investigation that compared the fluorescence of RPE of AMD and control donors but did not include nonuniform or ectopic cells.[19] Therefore, we found for RPE cells only marginal differences of the spectra in AMD and control eyes, in agreement with Marmorstein et al.,[24] and, in addition, significantly longer lifetimes. This is consistent with published in vivo findings by FLIO in patients with AMD, in whom long lifetimes were found in the outer ring of the Early Treatment Diabetic Retinopathy Study (ETDRS) grid.[25] In longitudinal studies, lengthening of lifetimes over AMD duration,[26] and lengthening of lifetimes and a hypsochromic shift of emission spectra in the process of RPE degeneration, comprising different steps of dysmorphia, hyperpigmentation, and migration, were observed.[7] However, FLIO does not provide depth resolution, and autofluorescence from different fundus layers is summed in these signals. This superposition of different fluorophores from different anatomic structures make it difficult to distinguish and characterize them without additional information. Therefore, insight into the fluorescence contributions of individual cells undergoing pathological alteration can be gained when in vivo observations are complemented by microscopy of tissue sections, as done in the current study.

Our current histologic findings complement our in vivo FLIO data and support the notion of a gradual change of the fluorophore composition or intracellular environment in RPE cells upon dysmorphia, degeneration, and migration despite the use of different excitation conditions (one-photon excitation in FLIO but two-photon excitation in histology) which give quantitatively different results (Supplementary Fig. S1). Interestingly, fluorescence changes go along with functional alterations and, possibly, molecular transdifferentiation of the cells indicated by immunohistochemistry. Thus, it might be speculated that the loss of immunoreactivity to RPE65 indicates that the cells cease the processing of retinoids. This, especially, may hold for cells migrated into the retina, where they no longer phagocytose photoreceptor outer segments. However, also the recycling of all-*trans* retinal to 11-*cis*-retinal, one of the key functions of RPE, might be ceased or at least reduced. This could explain the narrowing of the half-width of the emission spectrum along with a change of the emission maximum in autofluorescence lifetime. Interestingly, those deviations start already in the state of very nonuniform, bilaminar, and sloughed cells before intra-retinal migration. Thus, alterations of fluorescence properties might be an early indicator for functional insufficiency of RPE cells.

Investigations of the fine structure of RPE cells by volume electron microscopy revealed lipofuscin and melanolipofuscin granules in the apical 3/4 of cell bodies as well as mitochondria in the basal 3/4, occupying large fractions of the cell volume, whereas the apical processes are populated by melanosomes.[27] Further, using structured illumination microscopy (SIM), Bermond et al. identified nine different phenotypes of lipofuscin, melanin, and melanolipofuscin granules, showing hyper – or hypo-autofluorescence at 510 to 750 nm upon excitation at 488 nm.[28] Whereas the number of lipofuscin granules increased with age, that of melanolipofuscin did not change. Furthermore, Ach et al.[29] found differences in granule count for retinal areas defined by differences in rod:cone ratio (fovea, peri-fovea, and near periphery[30]). In AMD eyes, granule aggregation was observed in parallel with loss of autofluorescent granules, resulting in regions of high signal and no signal within the same cells, viewed en face.[29,31] As these investigations on RPE flatmounts used high-resolution microscopy without spectral or lifetime resolution, only fluorescence intensity could be observed. Bindewald-Wittich et al. showed for RPE flatmounts a 36-nm hypsochromic shift of fluorescence in cells with large lipofuscin granules with two-photon imaging with spectral resolution.[32] Similarly, Han et al. demonstrated a shift of autofluorescence to shorter wavelengths of large lipofuscin granules in dysmorphic (enlarged) RPE cells on RPE flatmounts in an 80-year-old subject.[33] Although we did not investigate single granules, the similarities in spectral changes in dysmorphic cells with a high load of lipofuscin might indicate that shorter emission wavelengths are associated with pathologic cell alterations. The observed hypsochromic shift of EMW by 10 to 20 nm over the development of pathology from very nonuniform RPE to intraELM cells agrees well with a highly significant 12 nm difference of the peak emission wavelength between aged healthy subjects and patients with AMD, observed in vivo by FLIO.[34]

Several pathways of RPE cell activation leading to complete RPE and outer retinal atrophy (cRORA), have been described by OCT and histology.[6,15,16] A healthy RPE layer shows polygonal cells of nearly uniform thickness. Cells may become nonuniform, slough off the continuous layer, and subsequently migrate into the retina. The abnormal RPE phenotypes are believed to be RPE and not phagocytes that ingested RPE, due to three lines of evidence[35–38]: (i) the close similarity of granule density to that of in-layer cells in high-resolution histology and electron microscopy, (ii) the lack of ultrastructural evidence to date for phagolysosomes as hallmarks of phagocytic activity, and (iii) the evidence from in vivo OCT for thickening of the RPE-basal lamina band followed by appearance of HRF directly above in the overlying retina.

From the expression of CD68, it might be argued that the intra-retinal cells, found here, are not RPE cells but phagocytes that have phagocytosed apoptotic RPE cells and are, therefore, pigmented. Thus, they could be microglia that migrated from the inner retina into the outer retina, monocyte-derived macrophages from the blood, or choroidal macrophages migrating into the retina. However, hyperpigmentation in CFP, which is associated with HRF in OCT and hyper-fluorescence, may persist over years in vivo.[7] In contrast, if these entities are phagocytes clearing apoptotic RPE, one might expect a disappearance of phagocytosed RPE cells as well as pigments over time. Furthermore, we see a gradual lengthening of lifetimes over the proposed stages of RPE dysmorphia, from in-layer to intra-ELM. Although not proof, because the current study examined a single time point only, these findings support our interpretation that we observed migrated and possibly transdifferentiated RPE cells.

For other cells to account for these phenomena, they would have to replicate both the quantitative aspects of the morphology as well as the behavior. We fully acknowledge that not all HRF are RPE. Imaging-histology correlations of eyes with neovascular AMD has identified other cell types, containing lipid droplets or heterogenous inclusions and

lacking abundant RPE organelles.[39,40] However, as the cells investigated herein were all highly pigmented, we consider them RPE-originated. The conversion of RPE from normal to abnormal is proposed to represent epithelial-mesenchyme transition (EMT), a well-studied process in cancer biology that includes metastasis and migration. Supporting this idea is the detection of markers for EMT in AMD eyes.[41–43] The current study adds to this idea by providing evidence of a transition in fluorescent properties in the same cellular phenotypes undergoing molecular changes demonstrated with immunohistochemistry. This pathway is associated with a monotonic decrease of the spectral emission maximum and an increase of the fluorescence lifetime. Possible reasons for the change of autofluorescence properties are discussed above.

On the other hand, cells may undergo apoptosis in situ, leaving behind shed fluorescent granules and dissociated cells. Whereas the shed granules do not change fluorescence spectra but do increase in lifetime (although not statistically testable), dissociated cells show similar properties (spectra as well as lifetimes) as very nonuniform cells, which is in line with an already shown risk for activation, migration, transdifferentiation, or apoptosis.[17] Another pathway of RPE fate is subduction under basal laminar deposits.[6] Although the number of subducted cells found here was too small for statistical comparison ($n = 5$), these cells showed the longest lifetimes and spectral peaks similar to that of intraretinal cells. Thus, it might be that these cells, which cease to contact photoreceptor outer segments or form junctions with other RPE, undergo similar functional changes as intraretinal cells. It even might be speculated that the reason of RPE migration towards the retina and toward the choroid is the same: cells seeking oxygen and nutrients.[7,44]

Of course, it would be interesting and important to know the observed fluorophores and their possible change in RPE pathology. However, the sample volume and preparation did not allow further chemical analysis needed for the isolation and identification of the fluorophores. Thus, any conclusion on that from our results would be highly speculative and is beyond the scope of the current study. A recent study by Kotnala et al.[45] identified and quantified four bis-retinoids in the RPE. Whereas N-retinyl-N-retinylidene ethanolamine (A2E), dihydropyridine phosphatidyl ethanolamine (A2DHPE), and monofuranA2E (MFA2E) was more abundant in eyes >60 years than eyes <60 years, A2-glycerophosphoethanolamine (A2GPE) did not show this difference, and all 4 were more abundant in peripheral retina than in the macula. Thus, the relative abundance of these or other bis-retinoids may differ among dysmorphic RPE. However, also a modification of the fluorophores themselves, for example, by oxidation, or a change in the intracellular milieu, could have altered the fluorescence properties.[46]

Overall, the independent measures fluorescence spectra and lifetime are both suitable to describe the changes of FAF. Whereas normally aged and bilaminar cells can be distinguished by their fluorescence lifetimes, intraPS and intraELM cells do not differ in lifetime but just in their spectral emission peak. Nevertheless, also those intraretinal cells can be distinguished by FLIM if the relative abundances (α%1–α%3 in the Supplementary Table S2) of the single fluorescence decay components are considered. Thus, extending lifetime analysis beyond the amplitude weighted means might give more detailed information in certain cases. In general, fluorescence lifetimes and spectra can be considered as complementary measures describing RPE alteration during AMD progression toward an atrophic state. Changes of FAF properties already were observed clinically by FLIO[7]; however, more research is needed to understand the biochemical milieu of the fluorescence alterations and their association with cellular function.

A strength of this study is the large number of cells analyzed per morphology. Because the number of available eyes was limited, and many cells came from two samples, it might be questioned whether our results are truly representative for all patients with AMD. Nevertheless, the results are in concordance with previous in vivo[7,13,25,26,34] and in vitro studies.[19,24,47,48] Some RPE lesions, such as shed granules and subducted cells, are clearly under-represented in our study. In addition, single cells within the uniform layer were not further characterized. Cao et al. found individual cells in the intact RPE layer already losing markers for retinoids and gaining markers for immune response.[17] Rudolf et al. showed that uniform RPE in geographic atrophy (GA) eyes, peripheral to the atrophy zone, resembled uniform RPE in aged-matched control eyes, but occasionally showed dips in autofluorescence emission intensity.[49] For future work, granule composition and autofluorescence of single cells, also in the uniform RPE layer of GA eyes, should be studied in more detail. In addition, bilaminar RPE layers could be re-examined in neovascular AMD eyes, where they are more common,[15] to allow better histologic and autofluorescence differentiation with cells such as sloughed at slightly different axial locations.

Another limitation of the study is the usage of paraformaldehyde-fixed tissue samples. This preserves tissue morphology better than sections of fresh-frozen tissue. On the other hand, fixation may interfere with the measured fluorescence properties, giving spectral maxima and lifetimes different from in vivo. However, the use of fixed tissues, which provide superior morphology, may be acceptable for studies of autofluorescence intensity and lipid composition.[49,50] In a previous investigation,[19] we found only marginal differences between lifetimes and spectral peaks, measured in fixed and fresh frozen tissue. Our technique does not allow visualization of metabolic markers like NADH and FAD that may greatly change postmortem. NADH is a minor contributor to fluorescence signals investigated in our study because it excites in UV; however, here we excited at a longer wavelength. FAD may contribute to FAF signal in vivo and be degraded in histology samples. Thus, we can focus on the fluorescent byproducts of interest without major interference by other fluorophores.

Finally, the results presented here are only qualitatively comparable with those of in vivo FLIO due to the use of two-photon excitation compared to one-photon excitation in FLIO. Although both investigations exhibit strikingly similar changes in fluorescence lifetimes and spectral peaks, the quantitative values differ. A possible reason, among others, may be a contribution of melanin fluorescence to signals generated by two-photon excitation.

In conclusion, herein, we showed changes of RPE fluorescence properties along the pathway from morphologies indicative of healthy aging to states of morphologic displacement and functional alteration. This confirms and further specifies previous in vivo investigations, using FLIO. As RPE changes, clinically seen as hyperpigmentation in color fundus photography and HRF in OCT, are known risk factors for the progression of AMD to the stage of geographic atrophy or cRORA, the according changes of fluorescence

spectra and lifetimes, reported here and in vivo,[7] might be considered as early risk markers and should be further investigated with respect to their etiology as well as their earliest clinical appearance.

Acknowledgments

Tissue acquisition and distribution was supported by NIH grant R01EY027948 (CAC).

Disclosure: **R. Simon**, None; **M. Jentsch**, None; **P. Karimimousivandi**, None; **D. Cao**, None; **J.D. Messinger**, None; **D. Meller**, None; **C.A. Curcio**, Apellis (C), Astellas (C), Boehringer Ingelheim (C), Genentech/Roche (P), Regeneron (P), Heidleberg Engineering (P); **M. Hammer**, None

References

1. Wong WL, Su X, Li X, et al. Global prevalence of age-related macular degeneration and disease burden projection for 2020 and 2040: a systematic review and meta-analysis. *Lancet Glob Health*. 2014;2:e106–e116.
2. Jonas JB, Cheung CMG, Panda-Jonas S. Updates on the Epidemiology of Age-Related Macular Degeneration. *Asia Pac J Ophthalmol (Phila)*. 2017;6:493–497.
3. Christenbury JG, Folgar FA, O'Connell RV, et al. Progression of intermediate age-related macular degeneration with proliferation and inner retinal migration of hyperreflective foci. *Ophthalmology*. 2013;120:1038–1045.
4. Nassisi M, Lei J, Abdelfattah NS, et al. OCT Risk Factors for Development of Late Age-Related Macular Degeneration in the Fellow Eyes of Patients Enrolled in the HARBOR Study. *Ophthalmology*. 2019;126:1667–1674.
5. Waldstein SM, Vogl WD, Bogunovic H, Sadeghipour A, Riedl S, Schmidt-Erfurth U. Characterization of Drusen and Hyperreflective Foci as Biomarkers for Disease Progression in Age-Related Macular Degeneration Using Artificial Intelligence in Optical Coherence Tomography. *JAMA Ophthalmol*. 2020;138:740–747.
6. Curcio CA, Zanzottera EC, Ach T, Balaratnasingam C, Freund KB. Activated Retinal Pigment Epithelium, an Optical Coherence Tomography Biomarker for Progression in Age-Related Macular Degeneration. *Invest Ophthalmol Vis Sci*. 2017;58:BIO211–BIO226.
7. Hammer M, Jakob-Girbig J, Schwanengel L, et al. Progressive Dysmorphia of Retinal Pigment Epithelium in Age-Related Macular Degeneration Investigated by Fluorescence Lifetime Imaging. *Invest Ophthalmol Vis Sci*. 2021;62:2.
8. Ly A, Nivison-Smith L, Assaad N, Kalloniatis M. Fundus Autofluorescence in Age-related Macular Degeneration. *Optom Vis Sci*. 2017;94:246–259.
9. Sahinoglu Keskek N, Sermet F. The Use of Fundus Autofluorescence in Dry Age-Related Macular Degeneration. *Turk J Ophthalmol*. 2021;51:169–176.
10. Dysli C, Wolf S, Berezin MY, Sauer L, Hammer M, Zinkernagel MS. Fluorescence lifetime imaging ophthalmoscopy. *Prog Retin Eye Res*. 2017;60:120–143.
11. Sauer L, Andersen KM, Dysli C, Zinkernagel MS, Bernstein PS, Hammer M. Review of clinical approaches in fluorescence lifetime imaging ophthalmoscopy. *J Biomed Opt*. 2018;23:1–20.
12. Sauer L, Vitale AS, Modersitzki NK, Bernstein PS. Fluorescence lifetime imaging ophthalmoscopy: autofluorescence imaging and beyond. *Eye (Lond)*. 2021;35:93–109.
13. Schultz R, Hasan S, Curcio CA, Smith RT, Meller D, Hammer M. Spectral and lifetime resolution of fundus autofluorescence in advanced age-related macular degeneration revealing different signal sources. *Acta Ophthalmol*. 2022;100(3):e841–e846.
14. Hammer M, Schultz R, Hasan S, et al. Fundus Autofluorescence Lifetimes and Spectral Features of Soft Drusen and Hyperpigmentation in Age-Related Macular Degeneration. *Transl Vis Sci Technol*. 2020;9:20.
15. Zanzottera EC, Messinger JD, Ach T, Smith RT, Freund KB, Curcio CA. The Project MACULA Retinal Pigment Epithelium Grading System for Histology and Optical Coherence Tomography in Age-Related Macular Degeneration. *Invest Ophthalmol Vis Sci*. 2015;56:3253–3268.
16. Zanzottera EC, Ach T, Huisingh C, Messinger JD, Spaide RF, Curcio CA. Visualizing Retinal Pigment Epithelium Phenotypes in the Transition to Geographic Atrophy in Age-Related Macular Degeneration. *Retina*. 2016;36(Suppl 1):S12–S25.
17. Cao D, Leong B, Messinger JD, et al. Hyperreflective Foci, Optical Coherence Tomography Progression Indicators in Age-Related Macular Degeneration, Include Transdifferentiated Retinal Pigment Epithelium. *Invest Ophthalmol Vis Sci*. 2021;62:34.
18. Schweitzer D, Schenke S, Hammer M, et al. Towards metabolic mapping of the human retina. *Microsc Res Tech*. 2007;70:410–419.
19. Schultz R, Gamage KCLK, Messinger JD, Curcio CA, Hammer M. Fluorescence Lifetimes and Spectra of RPE and Sub-RPE Deposits in Histology of Control and AMD Eyes. *Invest Ophthalmol Vis Sci*. 2020;61:9.
20. Chen L, Cao D, Messinger JD, et al. Histology and clinical imaging lifecycle of black pigment in fibrosis secondary to neovascular age-related macular degeneration. *Exp Eye Res*. 2022;214:108882.
21. Ouyang Y, Heussen FM, Hariri A, Keane PA, Sadda SR. Optical coherence tomography-based observation of the natural history of drusenoid lesion in eyes with dry age-related macular degeneration. *Ophthalmology*. 2013;120:2656–2665.
22. Klemm M, Schweitzer D, Peters S, Sauer L, Hammer M, Haueisen J. FLIMX: A Software Package to Determine and Analyze the Fluorescence Lifetime in Time-Resolved Fluorescence Data from the Human Eye. *PLoS One*. 2015;10:e0131640.
23. Zanzottera EC, Messinger JD, Ach T, Smith RT, Curcio CA. Subducted and melanotic cells in advanced age-related macular degeneration are derived from retinal pigment epithelium. *Invest Ophthalmol Vis Sci*. 2015;56:3269–3278.
24. Marmorstein AD, Marmorstein LY, Sakaguchi H, Hollyfield JG. Spectral profiling of autofluorescence associated with lipofuscin, Bruch's Membrane, and sub-RPE deposits in normal and AMD eyes. *Invest Ophthalmol Vis Sci*. 2002;43:2435–2441.
25. Sauer L, Gensure RH, Andersen KM, et al. Patterns of Fundus Autofluorescence Lifetimes In Eyes of Individuals With Nonexudative Age-Related Macular Degeneration. *Invest Ophthalmol Vis Sci*. 2018;59:AMD65–AMD77.
26. Schultz R, Hasan S, Schwanengel LS, Hammer M. Fluorescence lifetimes increase over time in age-related macular degeneration. *Acta Ophthalmol*. 2021;99:e970–e972.
27. Pollreisz A, Neschi M, Sloan KR, et al. Atlas of Human Retinal Pigment Epithelium Organelles Significant for Clinical Imaging. *Invest Ophthalmol Vis Sci*. 2020;61:13.
28. Bermond K, Wobbe C, Tarau IS, et al. Autofluorescent Granules of the Human Retinal Pigment Epithelium: Phenotypes, Intracellular Distribution, and Age-Related Topography. *Invest Ophthalmol Vis Sci*. 2020;61:35.
29. Ach T, Tolstik E, Messinger JD, Zarubina AV, Heintzmann R, Curcio CA. Lipofuscin redistribution and loss accompanied by cytoskeletal stress in retinal pigment epithelium of eyes with age-related macular degeneration. *Invest Ophthalmol Vis Sci*. 2015;56:3242–3252.

Investigative Ophthalmology & Visual Science

30. Curcio CA, Sloan KR, Kalina RE, Hendrickson AE. Human photoreceptor topography. *J Comp Neurol*. 1990;292:497–523.
31. Gambril JA, Sloan KR, Swain TA, et al. Quantifying Retinal Pigment Epithelium Dysmorphia and Loss of Histologic Autofluorescence in Age-Related Macular Degeneration. *Invest Ophthalmol Vis Sci*. 2019;60:2481–2493.
32. Bindewald-Wittich A, Han M, Schmitz-Valckenberg S, et al. Two-photon-excited fluorescence imaging of human RPE cells with a femtosecond Ti:Sapphire laser. *Invest Ophthalmol Vis Sci*. 2006;47:4553–4557.
33. Han M, Bindewald-Wittich A, Holz FG, et al. Two-photon excited autofluorescence imaging of human retinal pigment epithelial cells. *J Biomed Opt*. 2006;11:010501.
34. Schultz R, Schwanengel L, Klemm M, Meller D, Hammer M. Spectral fundus autofluorescence peak emission wavelength in ageing and AMD. *Acta Ophthalmol*. 2022;100(6):e1223–e1231.
35. Berlin A, Cabral D, Chen L, et al. Correlation of Optical Coherence Tomography Angiography of Type 3 Macular Neovascularization With Corresponding Histology. *JAMA Ophthalmol*. 2022;140:628–633.
36. Berlin A, Cabral D, Chen L, et al. Histology of type 3 macular neovascularization and microvascular anomalies in anti-VEGF treated age-related macular degeneration [published online ahead of print September 15, 2022]. *medRxiv preprint*, https://doi.org/10.1101/2022.09.13.22279910.
37. Chen KC, Jung JJ, Curcio CA, et al. Intraretinal Hyperreflective Foci in Acquired Vitelliform Lesions of the Macula: Clinical and Histologic Study. *Am J Ophthalmol*. 2016;164:89–98.
38. Balaratnasingam C, Messinger JD, Sloan KR, Yannuzzi LA, Freund KB, Curcio CA. Histologic and Optical Coherence Tomographic Correlates in Drusenoid Pigment Epithelium Detachment in Age-Related Macular Degeneration. *Ophthalmology*. 2017;124:644–656.
39. Li M, Dolz-Marco R, Messinger JD, et al. Clinicopathologic Correlation of Anti-Vascular Endothelial Growth Factor-Treated Type 3 Neovascularization in Age-Related Macular Degeneration. *Ophthalmology*. 2018;125:276–287.
40. Pang CE, Messinger JD, Zanzottera EC, Freund KB, Curcio CA. The Onion Sign in Neovascular Age-Related Macular Degeneration Represents Cholesterol Crystals. *Ophthalmology*. 2015;122:2316–2326.
41. Guidry C, Medeiros NE, Curcio CA. Phenotypic variation of retinal pigment epithelium in age-related macular degeneration. *Invest Ophthalmol Vis Sci*. 2002;43:267–273.
42. Ghosh S, Shang P, Terasaki H, et al. A Role for betaA3/A1-Crystallin in Type 2 EMT of RPE Cells Occurring in Dry Age-Related Macular Degeneration. *Invest Ophthalmol Vis Sci*. 2018;59:AMD104–AMD113.
43. Datta S, Cano M, Satyanarayana G, et al. Mitophagy initiates retrograde mitochondrial-nuclear signaling to guide retinal pigment cell heterogeneity [published online ahead of print August 13, 2022]. *Autophagy*, https://doi.org/10.1080/15548627.2022.2109286.
44. Kanow MA, Giarmarco MM, Jankowski CS, et al. Biochemical adaptations of the retina and retinal pigment epithelium support a metabolic ecosystem in the vertebrate eye. *Elife*. 2017;6:e28899.
45. Kotnala A, Senthilkumari S, Wu G, et al. Retinal Pigment Epithelium in Human Donor Eyes Contains Higher Levels of Bisretinoids Including A2E in Periphery than Macula. *Invest Ophthalmol Vis Sci*. 2022;63:6.
46. Hammer M, Richter S, Guehrs K-H, Schweitzer D. Retinal pigment epithelium cell damage by A2-E and its photoderivatives. *Mol Vis*. 2006;12:1348–1354.
47. Ben Ami T, Tong Y, Bhuiyan A, et al. Spatial and Spectral Characterization of Human Retinal Pigment Epithelium Fluorophore Families by Ex Vivo Hyperspectral Autofluorescence Imaging. *Transl Vis Sci Technol*. 2016;5:5.
48. Tong Y, Ben Ami T, Hong S, et al. Hyperspectral Autofluorescence Imaging of Drusen and Retinal Pigment Epithelium in Donor Eyes with Age-Related Macular Degeneration. *Retina*. 2016;36(Suppl 1):S127–S136.
49. Rudolf M, Vogt SD, Curcio CA, et al. Histologic basis of variations in retinal pigment epithelium autofluorescence in eyes with geographic atrophy. *Ophthalmology*. 2013;120:821–828.
50. Kotnala A, Anderson DMG, Patterson NH, et al. Tissue fixation effects on human retinal lipid analysis by MALDI imaging and LC-MS/MS technologies. *J Mass Spectrom*. 2021;56:e4798.

Investigative Ophthalmology & Visual Science